



Full Text View

[Volume 32, Issue 2 \(February 2002\)](#)

Journal of Physical Oceanography

Article: pp. 558–572 | [Abstract](#) | [PDF \(429K\)](#)

Idealized Models of Slantwise Convection in a Baroclinic Flow

Fiammetta Straneo*, Mitsuhiro Kawase, and Stephen C. Riser

School of Oceanography, University of Washington, Seattle, Washington

(Manuscript received March 13, 2000, in final form August 15, 2000)

DOI: 10.1175/1520-0485(2002)032<0558:IMOSCI>2.0.CO;2

ABSTRACT

Intermediate, or deep, convection in a baroclinic flow occurs along slanted paths parallel to the alongflow absolute momentum surfaces. These surfaces are principally tilted due to the vertical shear in velocity but can be further modified by a nonvertical axis of rotation. An inviscid Lagrangian parcel model, using realistic parameters, is utilized to illustrate, qualitatively, the different scenarios resulting from the combined action of inertial and gravitational forces acting on sinking parcels of dense fluid. More quantitative results are derived from a series of numerical experiments using a zonally invariant, high-resolution, nonhydrostatic model. Convection occurring in a flow with tilted absolute momentum surfaces will mix properties along these slanted surfaces. This implies that the fluid can retain a weak vertical stratification while overturning and also, more importantly, that the evolution of the convective layer cannot be described in terms of one-dimensional, vertical mixing. The authors show, for conditions typical of the Labrador Sea, that the convective layer depth difference between that estimated by mixing vertically and one obtained allowing for slantwise mixing can be greater than 100 m; slantwise convection reaches deeper because of the reduced stratification along the slanted paths. An alternative slantwise mixing scheme, based on the assumption of zero potential vorticity of the convected fluid, is proposed.

1. Introduction

Localized convection in the ocean is typically broken up into three distinct stages (following [Killworth 1979](#)): preconditioning, violent mixing, and breakup of the convected waters. The last two stages have been the focus of a series of laboratory and numerical simulations (e.g., [Jones and Marshall 1993](#); [Maxworthy and Narimousa 1994](#)) that have investigated the physics and derived parameterizations to be used in lower-resolution models. In the majority of these studies, a localized body of dense water is formed by the action of a localized surface buoyancy forcing (such as a disk of

Table of Contents:

- [Introduction](#)
- [The setting: The Labrador](#)
- [A Lagrangian model for](#)
- [Numerical simulations](#)
- [Implications for the](#)
- [Discussion](#)
- [REFERENCES](#)
- [APPENDIX](#)
- [TABLES](#)
- [FIGURES](#)

Options:

- [Create Reference](#)
- [Email this Article](#)
- [Add to MyArchive](#)
- [Search AMS Glossary](#)

Search CrossRef for:

- [Articles Citing This Article](#)

Search Google Scholar for:

- [Fiammetta Straneo](#)
- [Mitsuhiro Kawase](#)
- [Stephen C. Riser](#)

cooling) on an ocean initially at rest. The vigorous stirring by the convective cells, or plumes, which takes place in the violent mixing stage, is found to be well described by a one-dimensional vertical mixing scheme. The final collapse stage, on the other hand, is found to be primarily due to lateral stirring by eddies formed as a result of baroclinic instability of the rim current at the edge of the forced region (see [Visbeck et al. 1996](#)). While it has many advantages, localization of convection by imposing a localized buoyancy flux instead of using an initially preconditioned ocean has also led to the enhancement of some processes and diminished the importance of others. Lateral fluxes due to baroclinic instability may be among the enhanced processes, as argued by [Straneo and Kawase \(1999\)](#), since in any case of localized forcing the horizontal density gradient at the edge of the region of deep convection must grow in time, while there are many instances of preconditioned convection where it can decrease. Moreover, disk of cooling experiments tend to confine the horizontal density gradients to a narrow region at the edge of the disk, effectively limiting any importance of horizontal gradients on the convective overturning.

A number of recent studies have indicated that in the presence of a horizontal stratification convection can occur along slanted paths. Among these is that of [Haine and Marshall \(1998\)](#), who, while still using a horizontally varying forcing, allow it to vary smoothly over a distance. Their initial condition is still that of a stratified, horizontally homogeneous ocean. Haine and Marshall find that fluid is initially mixed vertically, as in all localized forcing experiments, but after the development of a horizontal density gradient (as a result of the spatially varying buoyancy flux) convection occurs along slanted paths in both their two- and three-dimensional nonhydrostatic simulations. Similar slantwise sinking is observed in one of the first nonhydrostatic simulations of preconditioned convection by [Legg et al. \(1998\)](#) in which a uniform buoyancy flux acts over a cyclonic eddy. In both studies slantwise sinking results in the formation of a region of zero potential vorticity but stable stratification, to be contrasted with the zero potential vorticity region with no vertical stratification formed in the localized forcing simulations. Though neither study focuses on the slantwise sinking process, in both cases the authors suggest that it results from symmetric instability, a process thought to play a role in the formation of rain- and cloud bands as well as squall lines in the atmosphere (e.g., [Emanuel 1983a,b](#)).

Because the experiments of Legg et al. and Haine and Marshall show that slantwise convection can occur in a typical oceanic convective regime, this raises the issue of whether parameterizations of convection derived in an “upright convection regime,” void of horizontal density gradients, are still valid in the presence of horizontal gradients. This is the question addressed in this study. Since we believe that the mechanism described in this study is relevant to a number of regions in the World Ocean, most of the discussion is in terms of parameters and is not specific to any particular region. However, to confirm that it is of relevance for a typical deep and intermediate convection regime, our examples use parameters derived from observations in the Labrador Sea, where a large quantity of data has recently been made available as a result of the Labrador Sea Deep Convection Experiment ([Lab Sea Group 1998](#)). A short description of these reference values is given in [section 2](#). First, in [section 3](#), we briefly review the physics of slantwise sinking by means of a Lagrangian parcel model following the methodology employed by [Emanuel \(1983b\)](#) for the atmospheric case. The horizontal component of rotation, which a number of authors ([Garwood 1991](#); [Denbo and Skillingstad 1996](#)) have already argued should not be neglected in simulations of oceanic convection, is retained in the model's formulation. This simple modeling approach serves the dual purpose of identifying the basic physical mechanisms and of highlighting some of the ocean/atmosphere differences. A more quantitative approach is achieved by means of a numerical, zonally invariant, high-resolution nonhydrostatic model ([section 4](#)). The fact that convection (and hence mixing) occurs along nonvertical paths has a number of important implications. Among these is that convection penetrates deeper during slantwise sinking than if simple upright convection occurred. This result and other implications are presented in [section 5](#), followed by a final discussion in [section 6](#).

2. The setting: The Labrador Sea

The parameter values for the analytical and numerical experiments described in this paper are taken from observations in the Labrador Sea region and are briefly outlined here. Let 60°N be a reference latitude for the whole region, which yields a Coriolis parameter of $f = 1.26 \times 10^{-4} \text{ s}^{-1}$ and a horizontal Coriolis parameter (see [appendix A](#)) $f^* = 0.73 \times 10^{-4} \text{ s}^{-1}$. The central Labrador Sea is characterized by a stratified surface layer with a typical buoyancy frequency of $8.5 \times 10^{-4} \text{ s}^{-1}$ and a deeper (to about 2000 m) weakly stratified region with a buoyancy frequency of $2.1 \times 10^{-4} \text{ s}^{-1}$ ([Lazier 1980](#)). More important to this study is the magnitude of the horizontal gradients during the winter. Analysis of the hydrographic data collected in the winter of 1996/97 (hereafter 1997) (courtesy of R. Pickart) has revealed the existence of two different regimes. The first is the boundary current regime: Both the Labrador and the Greenland Currents have horizontal density gradients of the order of $0.02\text{--}0.05 \text{ kg m}^{-3}$ over several kilometers, yielding a buoyancy gradient $b_y = 2\text{--}5 (\times 10^{-8} \text{ s}^{-2})$. The second regime is found in the interior (central) Labrador Sea, which is typically much more horizontally homogeneous, though the hydrographic data shows that horizontal gradients of the order of 0.01 kg m^{-3} over 10 km, that is, buoyancy gradients of $b_y = 10^{-8} \text{ s}^{-2}$, are not uncommon. This order of magnitude for gradients in the interior is further supported from observations of eddies swept past the Ocean Weather Station Bravo mooring in the central Labrador Sea ([Lilly and Rhines 2002](#)).

For the purpose of illustrating the dynamics of the interaction of convection with a horizontal stratification, our analysis is

mostly confined to the case of a linear horizontal and vertical stratification (with a constant buoyancy frequency of $3 \times 10^{-4} \text{ s}^{-1}$), which is within the observed range. For the horizontal stratification, except when noted otherwise, a reference horizontal buoyancy gradient of 10^{-8} s^{-2} is chosen. This choice, corresponding to gradients observed in the central Labrador Sea, is motivated by the fact that this is the region of deepest convection and also because a larger gradient would simply enhance the described effects. Finally, in the numerical experiments a surface buoyancy flux of $2 \times 10^{-7} \text{ m}^2 \text{ s}^{-3}$ is applied to the ocean's surface. Taking a typical thermal expansion coefficient of $9 \times 10^{-5} \text{ K}^{-1}$ for Labrador Sea wintertime conditions ($S = 34.7 \text{ psu}$ and $T = 3^\circ\text{C}$), this corresponds to a heat flux of approximately 800 W m^{-2} , within the observed range of $400\text{--}800 \text{ W m}^{-2}$ ([Lab Sea Group 1998](#)) and which allows formation of a convective layer of approximately 1000 m in three days, the typical duration of a winter storm.

3. A Lagrangian model for slantwise convection


In an attempt to explain the presence of banded features in precipitation and in clouds, a number of scientists have investigated two-dimensional (in the vertical) instabilities of the baroclinic atmosphere. A baroclinic geostrophic flow, assumed to be invariant in one direction, that is gravitationally and centrifugally (or inertially) stable can still be subject to a hybrid instability known as symmetric instability [see [Emanuel \(1994\)](#) for a review]. To understand symmetric instability consider a parcel of density ρ_0 and angular momentum m_0 within an adiabatic and inviscid flow. If the parcel is displaced from its equilibrium position, the inertial and gravitational forces will act to accelerate it horizontally and vertically, respectively, toward its neutral density and angular momentum surfaces. Under certain conditions of the mean flow and under displacements of a certain magnitude, the net acceleration may act to further displace the parcel from its initial equilibrium position ([Emanuel 1983b](#)). The necessary, and sufficient, condition for this to occur is that the potential vorticity of the mean flow be less than zero ([Hoskins 1974](#)). Since potential vorticity is conserved in the absence of friction and diabatic effects, the latter must be responsible for generating an instability in a previously stable system. In the atmosphere, the mechanism thought to be principally responsible for the creation of unstable regions is the reduction in static stability associated with latent heat release ([Bennetts and Hoskins 1979](#)), so the instability is referred to as “moist symmetric instability.”

Given the localized nature of the instability (it is confined to the unstable region) and the small Froude number associated with it, [Emanuel \(1983b\)](#) developed a parcel model to describe the dynamics of moist symmetric instability (also known as slantwise convection). Following this same methodology, we here present a Lagrangian parcel model to address the motion of an oceanic parcel of fluid convecting in a geostrophic, baroclinic flow. Though there is a number of similarities between moist symmetric instability and oceanic slantwise convection, there are also some important differences that make it instructive to reconsider the Lagrangian dynamics in the oceanic context. One such difference, which we will return to in the discussion, is that while the atmosphere has a mechanism (diabatic heating due to latent heat release) for generating unstable regions in its interior, in the ocean regions of negative potential vorticity can only be formed at the surface or other boundaries ([Haynes and McIntyre 1990](#)). Thus, while in the atmosphere parcel theory is utilized to determine the stability of a parcel, located in the interior, with respect to perturbations, in the ocean we are interested in the dynamics of a *gravitationally unstable parcel* whose motion is also influenced by rotational constraints. Another difference results from the relevance, in the oceanic case, of the rotational terms due to the tilt of the earth's axis of rotation with respect to the local gravity vector, which can be safely neglected in the atmospheric convection regime. A scaling argument for inclusion of these terms in the oceanic convective regime is given in [appendix A](#).

a. The model

Here we present results from a parcel model designed to capture the essential dynamics of convection in a baroclinic, geostrophic flow. A similar model has been used in the atmospheric context to describe the moist ascent of a two-dimensional air tube subject to moist symmetric instability ([Emanuel 1983b](#)). To represent the buoyancy loss to the atmosphere, the parcel, initially located at the surface, is denser than the surrounding fluid. Following [Emanuel's \(1983b\)](#) model, we make the assumption that the mean flow is unperturbed by the parcel's motion (equivalent to assuming a small Froude number) and that there is no mixing. As a result, the parcel's buoyancy is unmodified from its initial value and the only pressure gradient force the parcel is subject to is due to the mean flow. The geostrophic momentum balance in the zonal mean flow, assumed to be steady, is

$$-P_x = 0, \quad -P_y = fU, \quad -P_z = -B - f^*U,$$

where $B(y, z)$ is the buoyancy, $U(y, z)$ is the zonal velocity, P is the reduced pressure (pressure normalized by the reference density), subscripts indicate partial derivatives, and f^* is the horizontal Coriolis parameter ([appendix A](#)). A parcel of buoyancy b_0 is initially at the surface, embedded in this zonal flow (see [Fig. 1](#) ). In this zonally invariant scenario, one can define ([Emanuel 1983b](#)) an analog to angular momentum known as *zonal absolute momentum* (ZAM), which in this oceanic case also includes a contribution from the horizontal component of rotation:

$$m = u - fy + f^*z.$$

ZAM is a conserved quantity in the absence of viscosity and of external forces acting in the zonal direction. Let the mean flow properties be indicated by uppercase letters and the parcel's properties with lowercase letters so that the mean's flow ZAM is given by $M = U - fy + f^*z$. The Lagrangian equations of motion for the parcel, assuming no viscous or diffusive effects, can then be written as

$$\begin{aligned} \frac{dm}{dt} &= 0 & \frac{dv}{dt} &= f(M - m_0) = f\Delta m \\ \frac{dw}{dt} &= -(B - b_0) - f^*(M - m_0) \\ &= -\Delta b - f^*\Delta m, \end{aligned} \quad (1)$$

where u , v , and w are the Cartesian components of the parcel's velocities, and m_0 is the initial ZAM of the parcel. Because we are interested in capturing the dynamics of oceanic convection, we impose that the parcel's conserved buoyancy at its initial location, b_0 , is less than that of the mean flow (i.e., $\Delta b < 0$). The parcel is, therefore, initially displaced from its equilibrium position—that point in space where its buoyancy and ZAM coincide with those of the mean flow. The zonal part of the solution is less interesting because of the assumption of zonal invariance and is limited to an inertial oscillation in response to any velocity in the meridional or vertical directions. Finally, we limit our attention to mean flows with potential vorticity greater than zero,


$$PV = B_y(U_z + f^*) + B_z(f - U_y) > 0, \quad (2)$$

and that are therefore stable to gravitational, centrifugal, and symmetric instabilities.



b. Solution for a horizontally and linearly stratified mean flow

We present solutions for the simple case of a mean flow with a linear horizontal and vertical stratification:

$$\begin{aligned} B(y, z) &= \alpha y + N^2 z & U(y, z) &= -\frac{\alpha z}{f} \\ M(y, z) &= \left(f^* - \frac{\alpha}{f}\right)z - fy \end{aligned} \quad (3)$$

where α is the horizontal buoyancy gradient measured in s^{-2} and is referred to as *horizontal stratification*. Here we limit our discussion to a description of the parcel's trajectories, and the actual solutions are outlined in [appendix B](#). Since we are interested in the relative effects of a horizontal stratification and of a horizontal component of rotation, we examine different solutions for various combinations of f^* and α . When not zero, their values are set to those discussed in [section 2](#). The parcel's initial buoyancy (b_0) is set to be that of the mean flow at $y = 0$ and $z = 1000$ m. Trajectories (dotted) are plotted in time from $t = 0$ to $t = 5/f$ and overlaid on the isopycnals (solid) and ZAM surfaces (dashed) of the mean flow ([Fig. 2](#) ). The equilibrium point $[(y_p, z_p)$, [appendix B](#)] is indicated in the plots as an open circle.

1) NO HORIZONTAL STRATIFICATION: $\alpha = 0$

With no horizontal stratification, isopycnals are flat and ZAM surfaces are tilted only if $f^* \neq 0$. Vertical ZAM surfaces ($f^* = 0$) cause the parcel to sink vertically with no horizontal acceleration—the classic buoyancy oscillation ([Fig. 2a](#) ). When the exact same parcel sinks in a region where $f^* \neq 0$, its initially vertical acceleration displaces it from its equilibrium ZAM surface, causing it to be horizontally accelerated. This is an example of slantwise sinking entirely induced by the horizontal component of rotation ([Fig. 2b](#) ). The depth (z_p) of the equilibrium point is the same for both $f^* = 0$ and $f^* \neq 0$.

2) WITH A HORIZONTAL STRATIFICATION: $\alpha \neq 0$

A nonzero vertical shear in the zonal mean flow will also (as for the case $f^* \neq 0$) cause ZAM surfaces to become tilted

with respect to the vertical. Depending on the relative sign of the vertical shear and of the horizontal component of rotation, these two effects can be acting in the same or in opposite directions. Let us first consider the case with no horizontal component of rotation. In [Figs. 2c and 2e](#) we show the trajectories for both a positive and a negative vertical shear. The same mechanism that was discussed for the case $\alpha = 0$ and $f^* = 0$ causes the parcel to accelerate horizontally (toward its equilibrium m surface) as it sinks. However, in this scenario, since the acceleration moves the parcel toward lighter fluid, the equilibrium point ends up being *deeper* than it was for the cases with no horizontal stratification (even though the vertical stratification and the parcel's initial buoyancy anomaly are the same). Inclusion of the horizontal component of rotation in this horizontally stratified flow further modifies the picture. When these act in opposition, the tilt of the ZAM surfaces can be greatly reduced ([Fig. 2d](#); $\alpha, f^* > 0$). This is a case of weak or no slantwise convection, even though there is a vertical shear in the mean flow (vertical ZAM surfaces require $\alpha \approx f f^*$ and give rise to a buoyancy-oscillation-type solution such as that shown in [Fig. 2a](#), and at the same frequency). When the sign of the horizontal stratification is reversed, inclusion of the f^* terms tends to lower the potential vorticity (PV) of the mean flow by decreasing the angle between ZAM surfaces and isopycnals. In terms of parcel dynamics, the horizontal acceleration is greater than for the $f^* = 0$ case, and the equilibrium point is even deeper ([Fig. 2f](#)).

c. Conclusions from the analytical results

The analytical model, though clearly a crude representation of oceanic convection, is instrumental in illustrating how the ambient mean flow determines the path and depth of a sinking parcel. It shows how the trajectory of a sinking parcel is governed by the mean flow's ZAM surfaces. These are tilted, with respect to the vertical, if the absolute meridional vorticity of the mean flow is non-zero, which can occur from either (or both) a nonzero vertical shear in the mean flow (i.e., a horizontal stratification) or an axis of rotation that has a nonzero component in the horizontal direction perpendicular to the mean flow. The effect of a horizontal stratification associated with a vertical shear in the mean flow is to drive a parcel toward the lighter fluid as it sinks, while that of the horizontal component of rotation is to drive it south (north) in the Northern (Southern) Hemisphere. When acting together these mechanisms can clearly oppose or enhance each other.

The analytical model also showed that the path of the sinking parcel, as it finds its neutral density surface, is constrained along the mean flow's ZAM surface on which it was originally located. In the case of a horizontally stratified fluid, that the parcel is displaced toward lighter fluid causes it to find its neutral density surface at a *greater* depth than it would if it were to simply sink vertically.

4. Numerical simulations

After the qualitative description of [section 3](#), we here attempt to address the issue of when slantwise convection is important and what this implies with regard to convective parameterizations in a more realistic scenario.

a. The numerical model

The large range of time- and space scales involved in deep oceanic convection poses a difficult task to a modeler; hence, it is common for modelers to select one particular aspect of the problem and make some simplifying assumption about the remaining unresolved scales. Given that the focus of this study is the interaction of convection with a baroclinic geostrophic flow during the rapid overturning phase, we need to use a nonhydrostatic model capable of resolving the small-scale overturning cells and at the same time to be able to integrate over a domain large enough to include the large-scale flow. Because of the large computational costs involved we make two simplifying assumptions: that there are no variations in the zonal direction and that the subgrid unresolved processes can be parameterized in the form of a simple Fickian, constant coefficient diffusivity. The second assumption has been employed in a number of simulations of convection (e.g., [Jones and Marshall 1993](#); [Legg et al. 1998](#); [Haine and Marshall 1998](#)) and can be justified on the basis that plumes are the dominant mixing agents during deep convection as supported by higher-resolution simulations (e.g., [Denbo and Skvllinstad 1996](#)), by laboratory experiments (e.g., [Maxworthy and Narimousa 1994](#)), and by observations of plumelike events from moored instruments that have recorded deep convection events (e.g., [Schott et al. 1993](#); [Lilly et al. 1999](#)). The validity of the assumption of zonal invariance is discussed below.

The model used, then, is a nonhydrostatic, Boussinesq numerical model that assumes no variations in the zonal direction. In the usual notation the equations are

$$\begin{aligned}\frac{Du}{Dt} - fv &= \nu_v \frac{\partial^2 u}{\partial z^2} + \nu_h \frac{\partial^2 u}{\partial y^2} \\ \frac{Db}{Dt} &= \kappa_v \frac{\partial^2 b}{\partial z^2} + \kappa_h \frac{\partial^2 b}{\partial y^2} \\ \frac{D\xi}{Dt} &= f \frac{\partial u}{\partial z} + \frac{\partial b}{\partial y} + \nu_v \frac{\partial^2 \xi}{\partial z^2} + \nu_h \frac{\partial^2 \xi}{\partial y^2}\end{aligned}\quad (4)$$

where

$$\begin{aligned}\frac{D}{Dt} &= \frac{\partial}{\partial t} + v \frac{\partial}{\partial y} + w \frac{\partial}{\partial z}, & v &= -\frac{\partial \psi}{\partial z}, & w &= \frac{\partial \psi}{\partial y}, \\ \xi &= \nabla^2 \psi,\end{aligned}$$

$b = -g\rho' / \rho_0$ is buoyancy, and ν and κ are the eddy viscosity and diffusivity (subscripts indicate horizontal or vertical coefficients). The model uses a staggered grid with buoyancy and the zonal velocity defined at the center of the grid rectangle, the normal component of velocity at the sides, and vorticity and streamfunction at the corners. Similar to other nonhydrostatic simulations of deep convection (e.g., [Jones and Marshall 1993](#)) the Prandtl number is chosen to be 1 and the horizontal diffusivity used is $5 \text{ m}^2 \text{ s}^{-1}$. Because of the higher vertical resolution of this model we are able to use a lower vertical diffusivity, $\kappa_v = 0.03\text{--}0.06 \text{ m}^2 \text{ s}^{-1}$, than was used in these other experiments (ranging from 0.2 to $0.7 \text{ m}^2 \text{ s}^{-1}$).

This value is still large compared to observations but is required for the numerical stability of the model, given the comparatively large vertical velocities; nonetheless, it should be stressed that it is small enough that the diffusive timescale is much smaller than the vertical advective timescale of the plumes. Horizontal grid spacing is 125 m, vertical is 15 m, and the basin used is 50 km by 2000 m. Boundary conditions are no flux for buoyancy for the lateral and bottom boundaries, while the flux condition at the surface is given by $Q(y, t) = -\kappa_v \partial b / \partial z$. Boundary conditions for the momentum equations are no stress at all boundaries except for the bottom, which is no slip. An Adams–Bashforth time stepping scheme is used with a 30-s time step. [Smolarkiewicz's \(1983\)](#) advection scheme is used to limit the numerical diffusion of the advection scheme.

After a short adjustment time, a uniform buoyancy flux is applied at the surface of the model. The positive buoyancy flux (implying loss of buoyancy at the surface) causes the formation of an unstably stratified diffusive boundary layer at the surface. The thickness of this boundary layer grows in time until (after approximately a half day) convective plumes develop and start depleting dense fluid from the surface layer. Once the plumes develop, and as long as the buoyancy is being removed at the surface, the boundary layer thickness is maintained constant at a thickness of approximately 100 m, thus containing three to six grid points, depending on the vertical resolution used. Plumes that develop are approximately 500–1000 m in width and with typical vertical velocities of the order of $5\text{--}10 \text{ cm s}^{-1}$. These values are in good agreement with the observations of [Schott et al. \(1993\)](#) and with the vertical velocities measured by Lagrangian floats during sinking events ([Steffen and D'Asaro 2002](#)).

b. Effects on the individual plumes

In discussing this more complex model of convection one must depart from the parcel argument of the analytical model and instead consider the effects of a horizontal stratification and of a tilted axis of rotation on the convective cells, or plumes, which are driven by the surface buoyancy loss. Five experiments (expts 1–5) are designed to study the behavior of plumes in the presence of a horizontal stratification as well as a tilted rotation vector and to match the analytical cases presented in [section 3b](#). The common initial condition for all five is that of a linear vertical and horizontal stratification, $B(y, z) = N^2 z + \alpha y$, and of a geostrophic flow in thermal wind balance with the initial buoyancy distribution, $U(y, z) = -(z + H) \alpha / f$. The buoyancy flux applied, for a period of time T is spatially uniform in all experiments. Parameters are given in [Table 1](#).

- Experiment 1—Control experiment: the model is initialized with a horizontally homogeneous fluid of constant vertical stratification.
- Experiment 2—Effect of f^* : the initial and surface flux conditions are the same as for experiment 1, with the addition of a horizontal component of rotation.

- Experiment 3—Effect of a horizontal stratification: the model is initialized with a linear horizontal stratification superimposed on the same linear vertical stratification used in experiment 1, $f^* = 0$ in this experiment. Density is increasing to the south.
- Experiment 4—Coupling of f^* and of the horizontal stratification: same as experiment 3 (density increasing to the south) with the inclusion of f^* .
- Experiment 5—Coupling of f^* and of the horizontal stratification: same as experiment 4, only the sign of the horizontal stratification is reversed (density increasing to the north).

Snapshots of two adjacent plumes from each of the five experiments are shown in [Figs. 3a–e](#); these were all taken at the same time, three days after the buoyancy loss started. To compare the prediction of the analytical model to the numerical one we have overlaid, on each individual plume, a line corresponding to a ZAM surface of the mean flow; according to the analytical model prediction, the parcel's equilibrium point must lie on the same ZAM surface passing through its initial position. The length of this line is determined by assuming that the parcel's initial buoyancy, b_0 , is equal to that of the initial density of the ocean at the same location and at a depth h_{mix} ; where h_{mix} is the depth of the mixed layer that would form (under the assumption of vertical mixing only and nonpenetrative convection) when a buoyancy flux Q (the same as applied in the model) acts on the surface of the ocean for a time T equal to when the plume's snapshot was taken:

$$b_0 = B(y_0, z = -h_{\text{mix}}),$$

where

$$h_{\text{mix}} = \left(\frac{2QT}{N^2} \right)^{1/2}$$

and h_{mix} is derived in [Turner \(1973\)](#). If the parcel were to fall vertically, h_{mix} would be the depth of the equilibrium point at time T . Plumes in a horizontally homogeneous ocean where the axis of rotation is parallel to gravity, experiment 1, are vertically symmetric ([Fig. 3a](#)). In the analytical model this run corresponds to the trajectory illustrated in [Fig. 2a](#), the buoyancy oscillation. When the axis of rotation is tilted with respect to gravity, experiment 2, plumes tilt to the south with increasing depth ([Fig. 3b](#)) along the now tilted ZAM surfaces and in agreement with the analytical analog shown in [Fig. 2b](#). A shear in the mean flow with $f^* = 0$ will still cause ZAM surfaces to be nonvertical so that in experiment 3 plumes bend toward the lighter fluid with depth. Once again, the tilt in the plumes shows good agreement with the prediction of the analytical model (see [Fig. 2c](#)). The coupling of the effect due to a vertical shear and to a nonvertical axis of rotation is illustrated in experiments 4 and 5 ([Figs. 3d,e](#)). Parameters for experiment 4 are the same as those chosen for the trajectory shown in [Fig. 2d](#), where the summing of the two effects results in mutual almost complete cancellation. For this case convection is practically vertical. The summation of the two effects is shown in experiment 5. Plumes are much more tilted than in experiment 3, in the same way that the equilibrium point for the analytical solution shown in [Fig. 1f](#) is further removed from the origin than for the case shown in [Fig. 1e](#).

In general, there is excellent agreement between the theory developed in the analytical calculations and the numerical model's behavior. The plumes are essentially parallel to the mean flow's ZAM surfaces, and the depth to which they extend varies depending on their mean tilt. The implication is that the dynamical regime identified in the analytical solution is also valid, to leading order, in this fully nonlinear, diffusive, and viscous model.

5. Implications for the ocean

a. Tilt in the absolute momentum surfaces

The analytical theory, together with the numerical experiments, shows that, to leading order, convection occurs along ZAM surfaces. Here we evaluate what implications this finding has in terms of the depth and structure of the resulting convective layer. First, we estimate the typical tilt of ZAM surfaces in the Labrador Sea to show that these can considerably deviate from being vertical in regions characterized by a horizontal stratification. Next we consider the effects on the convective layer.

Taking a horizontal stratification and Coriolis parameters typical for the central Labrador Sea ([section 2](#)) and assuming a linear horizontal stratification, the angle that ZAM surfaces make to the vertical, θ , is



$$\tan\theta = \frac{M_y}{M_z} = \frac{f^*}{f} - \frac{\alpha}{f^2} = 0.58 \pm 0.63$$

$$= \begin{cases} 1.21 & \text{for } b_y < 0 \\ -0.05 & \text{for } b_y > 0. \end{cases}$$

Depending on the sign of α for every 1000 m of vertical sinking the parcel can also be displaced 1210 m to the north or 50 m to the south. This example serves the purpose of illustrating two facts for typical central Labrador Sea conditions. First, ZAM surfaces can be considerably tilted (with aspect ratio of order 1) due to either a horizontal stratification or the horizontal component of rotation. Second, the two effects can be of comparable magnitudes, which can result in a mutual cancellation or a doubling of the effects. In the boundary region, not surprisingly, ZAM surfaces are much more tilted, and, if we take a typical buoyancy gradient of order $3 \times 10^{-8} \text{ s}^{-2}$, we expect the aspect ratio (horizontal to vertical) of the convectively induced mixing to be of order 2 (this is without including the effects of f^*). In general, for strong horizontal gradients the effects of the horizontal component of rotation will become less and less important. Finally, all the examples and model simulations discussed until now have been for the case of a geostrophic zonal flow. These results can, however, be easily generalized for the case of a flow in any direction, provided that the absolute momentum surfaces considered are the *alongflow* ones [see [Straneo \(1999\)](#) for a derivation].

b. Implications for the convective layer depth

A variety of different parameterizations for deep convection are currently utilized in models that cannot resolve the process. Static instability is typically removed via a convective adjustment scheme that mixes density vertically until a neutral vertical stratification is reached, either instantaneously or over a finite period of time, (e.g., [Marotzke 1991](#)). Such a scheme is often included in a mixed layer model, which also accounts for the restratification of the layer (due to surface fluxes) as well as the entrainment at its base due to the unresolved turbulent kinetic energy (e.g., [Kraus and Turner 1967](#)). Alternative mixing schemes include those where density is mixed only when the Richardson number falls below a certain critical value [see [Large et al. \(1994\)](#) for a review]. Finally, because most of these parameterizations were developed for shallow mixed layers and not for deep convection regions, a number of *plume models* have been developed to better account for the fact that mixing during deep convection is predominantly due to the action of convective plumes (see [Paluskiewicz and Romea 1996](#), and references therein). In all of the above parameterizations mixing is always a vertical process. Yet we showed that plumes, the primary mixing agents during deep convection, are tilted with respect to the vertical axis when convection occurs in the presence of a horizontal stratification, implying that mixing occurs at an angle with the vertical. To be consistent with our numerical simulations, which, although nonhydrostatic, do not employ any sophisticated closure scheme, we confine our attention to the mixing of buoyancy only (essentially to the convective adjustment process) and assume convection to be nonpenetrative. Our goal is to show, in a simple context, how the slant in the mixing path needs to be taken into account. The inclusion of slantwise effects (and their interaction) with more sophisticated mixing models still needs to be investigated with more complex models.

Consider the case of a horizontally and vertically stratified ocean of initial buoyancy $B_o(y, z)$ subject to a uniform surface buoyancy flux Q switched on at time $t = 0$ ([Fig. 4a](#) ). For the sake of comparison we first consider vertical mixing alone and then discuss how slantwise mixing can be accounted for. If we assume convection to be vertical and nonpenetrative and buoyancy to be continuous at the base of the mixed layer ([Fig. 4b](#) ), then we can describe the buoyancy distribution at time t as

$$B(y, z, t) = \begin{cases} \bar{B}(y, t) & \text{for } z \geq -h_v(y, t) \\ B_o(y, z) & \text{for } z \leq -h_v(y, t). \end{cases} \quad (5)$$

Using [\(5\)](#) and conservation of buoyancy

$$\int_{-h_v}^0 \bar{B}(y, t) dz - \int_{-h_v}^0 B_o(y, z) dz = -Qt, \quad (6)$$

one can solve for h_v . For simplicity we consider the special case of an initial buoyancy distribution, $B_o(y, z) = \alpha y + g(z)$, where $g(z)$ represents a generic vertical buoyancy stratification. In the case of one-dimensional vertical mixing then, the horizontal gradient is unaffected by the buoyancy loss, and $\bar{B}(y, t)$ must be of the form $\bar{B}(y, t) = \alpha y + \bar{b}(t)$; by imposing buoyancy continuity at h_v we have $\bar{b}(t) = g(-h_v)$. Thus, [\(6\)](#) reduces to

$$h_v g(-h_v) - \int_{-h_v}^0 g(z) dz = -Qt, \quad (7)$$

and it is easy to show that for the case of linear vertical stratification, $g(z) = N^2 z$, it reduces to [Turner's \(1973\)](#) result:

$$h_v(t) = \sqrt{\frac{2Qt}{N^2}}. \quad (8)$$

We now consider the convective layer formed as a result of slantwise convection. Instead of assuming a vertically homogeneous mixed layer, we assume that the fluid is mixed along ZAM surfaces to form a layer of depth $h_s(y, t)$ characterized by zero PV (i.e., in which isopycnals are parallel to ZAM surfaces; [Fig. 4c](#) \Rightarrow). We use the same initial condition as above, $B_o(y, z) = \alpha y + g(z)$, with an associated thermal wind flow $U(y, z) = -\alpha z/f + U_o$, where U_o is a constant, and initial ZAM $M_o = -\alpha z/f + U_o - fy + f^*z$. We assume that the horizontal stratification remains unvaried as a result of convection (a reasonable assumption since there are no horizontal inhomogeneities to alter such a gradient) and that the flow remains in geostrophic balance so that the ZAM surfaces are unaltered by convection (an assumption confirmed by our numerical simulations). The slantwise convective layer formed as a result of convection can then, in analogy to [\(5\)](#), be written as

$$B(y, z, t) = \begin{cases} \bar{B}(y, z, t) & \text{for } z \geq -h_s(y, t) \\ B_o(y, z) & \text{for } z \leq -h_s(y, t). \end{cases} \quad (9)$$

If the horizontal stratification is unvaried, it follows that $\bar{B}(y, z, t)$ must be of the form $\bar{B} = \alpha y + n(z, t)$, and by imposing that isopycnals be parallel to the (unchanged) ZAM surfaces in the convected fluid one can derive \bar{B}_z :

$$\bar{B}_z = \bar{B}_y \frac{M_z}{M_y} = \alpha \frac{(\alpha - ff^*)}{f^2}.$$

Since the vertical stratification in the convective layer is independent of depth, it follows that $\bar{B}(y, z, t)$ must be of the form $\bar{B}(y, z, t) = \alpha y + \lambda z + c(t)$, where

$$\lambda = \frac{\alpha}{f} \left(\frac{\alpha}{f} - f^* \right) \quad (10)$$

is the vertical stratification in the convective layer. By imposing continuity of buoyancy at the base of the convective layer one finds $c(t) = g(-h_s) + \lambda h_s$, which accounts for the change in buoyancy at the surface. Finally, since there can be no net horizontal convergence/divergence of buoyancy due to convection, the depth to which mixing has modified the fluid can be calculated by applying the same vertically integrated conservation of buoyancy as in [\(6\)](#). For the initial buoyancy distribution described above, this becomes

$$\frac{\lambda h_s^2}{2} + h_s g(-h_s) - \int_{-h_s}^0 g(z) dz = -Qt. \quad (11)$$

Note that only cases of $\lambda > 0$ are physically acceptable, which implies $\alpha(\alpha - ff^*) > 0$. This is true (in the Northern Hemisphere) for all cases of negative α and for cases of positive α , provided that $\alpha > ff^*$. For $\alpha < ff^*$ with $\alpha > 0$, conservation of absolute momentum tends to result in a centrifugally unstable profile, which must then further overturn. In this case, then, the vertical mixing scheme would still hold. From here on, we will assume that $\lambda > 0$.

To understand the effects of slantwise convection, it is instructive to consider the case of an initially constant vertical stratification, $g(z) = N^2 z$. By solving [\(11\)](#) for this particular choice of $g(z)$, one obtains

$$h_s(t) = \sqrt{\frac{2Qt}{N^2 - \lambda}}. \quad (12)$$

Note that (8) and (12) are formally identical: twice the amount of buoyancy extracted divided by the stratification along the (slanted) path. The denominator of (12) is positive, provided that the PV of the mean flow is positive.

From comparing the two conservation equations, (7) and (11), one can deduce that the depth of slantwise mixing is always greater than that of vertical mixing. This can be intuitively explained by considering that as a result of slantwise convection fluid crosses fewer isopycnals per unit distance than during vertical mixing and therefore needs to penetrate deeper given the same buoyancy loss. This agrees with the deeper equilibration depth shown in Figs. 2c–f. In the absence of a horizontal stratification ($\alpha = 0$) $h_s = h_v$; though sinking can still occur at an angle with the vertical due to f^* , it does not encounter a different stratification due to its slanted path and, hence, the convective layer depth is equal to the vertical mixed layer depth (Fig. 2b).

To estimate the order of magnitude error associated with the assumption of vertical mixing in cases of slantwise convection, consider the case of linear horizontal stratification, with $\alpha = 2 \times 10^{-8} \text{ s}^{-2}$ and a vertical stratification representative of the Labrador Sea prior to deep convection (see Lazier 1980):

$$B_o(y, z) = \alpha y + N_1^2 z + N_2^2 L_z e^{z/L_z}$$

$$U_o(y, z) = -\frac{\alpha}{f}(z + H)$$

(see Table 1, expt 6, for the parameters utilized). The value for the surface stratification is slightly less than the observed mean, consistent with the idea that the deepest convection occurs in a preconditioned region. The vertical mixing depth obtained by solving (7) is $h_v = 836 \text{ m}$, while the slantwise convective layer depth from (11) is

$$h_s = \begin{cases} 895 \text{ m} & \text{for } \alpha > 0 \\ 1059 \text{ m} & \text{for } \alpha < 0. \end{cases}$$

The slantwise mixing predicted value is greater in both cases and, in particular, for the case where the effects of α and f^* couple. The slantwise convection scheme prediction is tested with the numerical model in experiment 6. The depth of the convective layer, while the fluid is still overturning, is shown in Fig. 5 by plotting the horizontally averaged density anomaly $\rho(y, z, t = 3.5) - \rho(y, 700, 0)$. The horizontal average (over the interior 40 km) is necessary to filter the plume noise and thus obtain a mean depth for the convective layer. The mean density profile in the numerical simulation compared to both the vertical and slantwise schemes' prediction confirms that slantwise convection has resulted in deeper than vertical convection in agreement with the slantwise scheme prediction (Fig. 5).

c. Convection in a geostrophic flow

The effects of slantwise convection are best summarized by considering the problem of convection in a localized baroclinic geostrophic flow. Note that, according to the theory developed above, upright convection will not be modified by a background barotropic flow since such a flow does not affect the tilt of the absolute momentum surfaces. We investigate convection in a particular baroclinic, meridional flow, the vertical shear of which is invariant with depth, experiment 7. The initial buoyancy and zonal velocity fields are given by

$$b_0(y, z) = N_1^2 z + N_2[1 + \tanh(y/L_y)]$$

$$u_0(y, z) = -\frac{N_2(z + H)}{fL_y \cosh^2(y/L_y)}$$

and are shown in Fig. 6a; the experiment's parameters are given in Table 1. According to (5) and (6), given any initial condition of the form $B_0(y, z) = s(y) + g(z)$, vertical mixing will not induce a variation in the horizontal stratification. Furthermore, since $g(z)$ is spatially invariant the vertical mixing model predicts that the mixed layer depth should not vary across the front, with h_v given by (8).

The initial ZAM distribution (Fig. 6b) shows how these surfaces are only tilted in the frontal region, due to the vertical shear in the flow, and hence we expect convection to be nonvertical in this region only. Moreover, since slantwise convection penetrates deeper than vertical convection, we expect the convective layer depth to vary across the front. These conclusions are confirmed in experiment 7 in terms of both the plumes' characteristics and the redistribution of buoyancy. Deeper plume penetration in the frontal region can be seen in the time-averaged kinetic energy in the vertical y - z plane, which essentially reflects the plumes activity (Fig. 6e). Similarly, the PV distribution shows how the region with approximately zero PV (a tracer for the depth of the convective layer) extends deeper at the front (Fig. 6f).

d. When is slantwise convection important?

We have shown that, in general, convecting parcels of fluid will tend to follow absolute momentum surfaces. This fact alone, however, does not necessarily imply a deeper convective layer. From the expression derived for the slantwise mixing depth, we can deduce that the slantwise mixing depth, h_s , will differ from the vertical mixing depth, h_v , only if the vertical stratification and λ [as defined in (10)] are of the same order of magnitude. If we neglect the effects of f^* , this implies that the depth of the convective layer will sensibly change only if $N^2 \approx a^2/f^2$ or, in physical terms, if the stratification along absolute momentum surfaces is effectively different from N^2 . In general, this will only hold in baroclinic flows that are weakly stratified. Note that even though this criterion is based on the slantwise mixing scheme derived for a particularly simple baroclinic flow, because it is a local criterion it can be used locally in any given flow. In terms of parameterizations of convection then, we suggest that this criterion be used to determine the degree of modification of the convective layer that slantwise effects can introduce. If it is significant, the scheme should be designed to mix along the local absolute momentum surfaces.

6. Discussion

In this study we have addressed the problem of convection in a horizontally stratified fluid. The horizontal component of rotation, often neglected in studies of convection, has also been included. Our results show that the joint action of gravitational and inertial forces causes convection to occur along slanted paths, parallel to the alongflow absolute momentum surfaces. These surfaces can be tilted due to either a shear in the geostrophic current (i.e., a horizontal stratification) or a nonvertical axis of rotation. The dynamics of slantwise convection is elucidated with a Lagrangian, analytical parcel model, following the same methodology employed by Emanuel (1983b) in addressing moist symmetric instability in the atmosphere. These results are validated by a series of experiments conducted with a nonhydrostatic, high-resolution, zonally invariant, numerical model. While there are many similarities between moist symmetric instability and what we have described as slantwise oceanic convection, there are also some important differences. In the atmosphere, interior regions with negative potential vorticity, susceptible to symmetric instability, can be generated via diabatic heating. Typically, then, studies of this phenomenon have concentrated on the evolution of regions that are symmetrically unstable though gravitationally and centrifugally stable (see, e.g., Jones and Thorpe 1992). In the interior of the ocean there is no mechanism equivalent to diabatic heating for generating regions of negative potential vorticity. Instead, this “oceanic” form of symmetric instability is essentially gravitational instability modified by inertial forces.

A first conclusion of this study is that these processes are relevant within a realistic parameter range, specifically the regime of the central Labrador Sea in the wintertime. Moreover, the horizontal component of rotation can play a significant role in increasing or reducing the slant angle due to a horizontal stratification. In the absence of a horizontal stratification, the horizontal component of rotation can still drive nonvertical convection. However, since there are no horizontal gradients, there is no net horizontal buoyancy flux, and, though convection is slantwise, this does not affect the depth of the convective layer.

An important implication of these results is that in the presence of a horizontal stratification the classic idea of mixed layer formation due to convection no longer holds. Because fluid sinks slantwise, it can convectively overturn while retaining a stable vertical stratification. In this case one should not expect to observe a vertically mixed layer by means of a vertically profiling measurement. Even more important is that a modification in the path of mixing (slanted as opposed to vertical) leads to a change in the depth to which convection occurs. This can be explained in terms of the different stratification encountered by plumes along their mixing path. We show that the assumption of vertical mixing (used in most nonpenetrative convective adjustment schemes) for convection in a sheared flow can lead to a significant error in the estimate of the convective layer depth. Instead of assuming vertical mixing we propose an alternative model for calculating the convected fluid's vertical extent. The model is based on the assumption of zero PV of the fluid once convection has occurred but allows for the fluid to be stably stratified. In terms of a simple baroclinic, localized front we show that convection can reach deeper within the front than in the surrounding fluid.

A number of important assumptions were made in this study. First of all, the flow is assumed to be invariant in one horizontal direction, which makes the alongflow absolute momentum surfaces material surfaces. The underlying assumption is that variations in one direction are much larger than variations in the perpendicular direction. This obviously finds a better application in boundary currents and frontal systems as opposed to eddies. Also, three-dimensional processes such as

baroclinic instability are not resolved and their coupling with slantwise convection processes needs to be determined. Moreover, we were able to calculate a slantwise mixing depth only for the particular case of a horizontal stratification that is spatially invariant. When this is no longer the case, convection will drive a change in the horizontal stratification that, in turn, will modify the alongflow absolute momentum surfaces. Though convection will still occur along these surfaces and still result in a region of zero PV with a stable vertical stratification, the computation of the convective layer depth is no longer analytically treatable. In terms of convective adjustment schemes, we suggested a criterion and speculated on how this effect could be included in parameterizations of convection.

Finally, the Lagrangian dynamics finds a natural application to vertically moving floats released in horizontally stratified regions, such as those of [Steffen and D'Asaro \(2002\)](#). This study suggests that, in the presence of a horizontal density gradient, these floats will sink, and thus profile, at angle with the vertical. Unfortunately, there is not enough data to verify that the Lagrangian floats were undergoing slantwise convection at any given time (E. Steffen 1999, personal communication). An attempt ([Straneo 1999](#)) made to compare Lagrangian float measurements with Eulerian ones from the hydrographic data, both taken in the same region during convection, shows that the variability in potential temperature observed by the floats is one order of magnitude smaller than that observed during the CTD profiles. This is consistent with the hypothesis of sinking along nonvertical paths.

Acknowledgments

The authors would like to thank E. D'Asaro, C. Bretherton, and J. Lilly for a series of fruitful discussions, and R. Pickart for providing the hydrographic data. All the numerical output figures were produced using FERRET, developed by Steve Hankin, and others, at PMEL.

References

- Bennetts D. A., and B. J. Hoskins, 1979: Conditional symmetric instability—A possible explanation for frontal rainbands. *Quart. J. Roy. Meteor. Soc.*, **105**, 945–962. [Find this article online](#)
- Denbo W., and E. D. Skyllingstad, 1996: An ocean large-eddy simulation model with application to deep convection in the Greenland Sea. *J. Geophys. Res.*, **101**, 1095–1110. [Find this article online](#)
- Emanuel K. A., 1983a: On assessing local conditional symmetric instability from atmospheric soundings. *Mon. Wea. Rev.*, **111**, 2016–2033. [Find this article online](#)
- Emanuel K. A., 1983b: The Lagrangian parcel dynamics of moist symmetric instability. *J. Atmos. Sci.*, **40**, 2368–2376. [Find this article online](#)
- Emanuel K. A., 1994: *Atmospheric Convection*. Oxford University Press, 580 pp.
- Garwood R. W., 1991: Enhancements of deep turbulent entrainment. *Deep Convection and Deep Water Formation in the Oceans*, P. C. Chu and J. C. Gascard, Eds., Elsevier, 197–214.
- Gascard J. C., and R. A. Clarke, 1983: The formation of Labrador Sea Water. Part II: Mesoscale and smaller-scale processes. *J. Phys. Oceanogr.*, **13**, 1779–1797. [Find this article online](#)
- Haine T. W. N., and J. Marshall, 1998: Gravitational, symmetric, and baroclinic instability of the ocean mixed layer. *J. Phys. Oceanogr.*, **28**, 634–658. [Find this article online](#)
- Haynes P. H., and M. E. McIntyre, 1990: On the conservation and impermeability theorems for potential vorticity. *J. Atmos. Sci.*, **47**, 2021–2031. [Find this article online](#)
- Hoskins B. J., 1974: The role of potential vorticity in symmetric stability and instability. *Quart. J. Roy. Meteor. Soc.*, **100**, 480–482. [Find this article online](#)
- Jones H., and J. Marshall, 1993: Convection with rotation in a neutral ocean: A study of open-ocean deep convection. *J. Phys. Oceanogr.*, **23**, 1009–1039. [Find this article online](#)
- Jones S. C., and A. J. Thorpe, 1992: The three-dimensional nature of “symmetric” instability. *Quart. J. Roy. Meteor. Soc.*, **118**, 227–258. [Find this article online](#)
- Killworth P. D., 1979: On chimney formations in the ocean. *J. Phys. Oceanogr.*, **9**, 531–554. [Find this article online](#)
- Kraus E. B., and J. S. Turner, 1967: A one-dimensional model of the seasonal thermocline. II. The general theory and its consequences.

Lab Sea Group, 1998: The Labrador Sea Deep Convection Experiment. *Bull. Amer. Meteor. Soc.*, **79**, 2033–2058. [Find this article online](#)

Large W., J. McWilliams, and S. Doney, 1994: Ocean vertical mixing: A review and a model with a non-local boundary layer parameterization. *Rev. Geophys.*, **32**, 336–403. [Find this article online](#)

Lazier J. R. N., 1980: Oceanographic conditions at O. W. S. Bravo 1964–1974. *Atmos.–Ocean*, **18**, 227–238. [Find this article online](#)

Legg S., J. McWilliams, and J. Gao, 1998: Localization of deep ocean convection by a mesoscale eddy. *J. Phys. Oceanogr.*, **28**, 944–970. [Find this article online](#)

Lilly J. M., and P. B. Rhines, 2002: Coherent eddies in the Labrador Sea observed from a mooring. *J. Phys. Oceanogr.*, **32**, 585–598. [Find this article online](#)

Lilly J. M., P. B. Rhines, M. Visbeck, R. Davis, J. R. N. Lazier, F. Schott, and D. Farmer, 1999: Observing deep convection in the Labrador Sea during winter 1994/95. *J. Phys. Oceanogr.*, **29**, 2065–2098. [Find this article online](#)

Marotzke J., 1991: Influence of convective adjustment on the stability of the thermohaline circulation. *J. Phys. Oceanogr.*, **21**, 903–907. [Find this article online](#)

Maxworthy T., and S. Narimousa, 1994: Unsteady, turbulent convection into a homogeneous, rotating fluid, with oceanographic applications. *J. Phys. Oceanogr.*, **24**, 865–887. [Find this article online](#)

Paluszkiwicz T., and R. D. Romea, 1997: A one-dimensional model for the parametrization of deep convection in the ocean. *Dyn. Atmos. Oceans*, **26**, 95–130. [Find this article online](#)

Schott F., M. Visbeck, and J. Fischer, 1993: Observations of vertical currents and convection in the central Greenland Sea during the winter of 1988–1989. *J. Geophys. Res.*, **98**, 14402–14421. [Find this article online](#)

Smolarkiewicz P. K., 1983: Simple positive definite advection scheme with small implicit diffusion. *Mon. Wea. Rev.*, **111**, 479–486. [Find this article online](#)

Steffen E. L., and E. A. D'Asaro, 2002: Deep convection in the Labrador Sea as observed by Lagrangian floats. *J. Phys. Oceanogr.*, **32**, 475–492. [Find this article online](#)

Straneo F., 1999: Dynamics of rotating convection including a horizontal stratification and wind. Ph.D. thesis. University of Washington, 150 pp.

Straneo F., and M. Kawase, 1999: Comparisons of localized convection due to localized forcing and to preconditioning. *J. Phys. Oceanogr.*, **29**, 55–68. [Find this article online](#)

Turner J. S., 1973: *Buoyancy Effects in Fluids*. Cambridge University Press, 367 pp.

Visbeck M., J. Marshall, and H. Jones, 1996: Dynamics of isolated convective regions in the ocean. *J. Phys. Oceanogr.*, **26**, 1721–1734. [Find this article online](#)

APPENDIX A

7. The Horizontal Component of Rotation

In a local Cartesian coordinate system (x, y, z) the earth's angular velocity, Ω , can be decomposed into a y and z component, such that $2\Omega = (0, f^*, f)$ where $f = 2\Omega \sin\phi$ and $f^* = 2\Omega \cos\phi$. The Boussinesq, nonhydrostatic equations of motion in the absence of external forces are

$$\frac{Du}{Dt} - fv + f^*w = -p_x + F^x$$

$$\frac{Dv}{Dt} + fu = -p_y + F^y$$

$$\frac{Dw}{Dt} - f^*u = -p_z - b + F^z, \quad (\text{A1})$$

where subscripts indicate partial derivatives, p is the reduced pressure, and $b = -g\rho' / \rho_0$ is buoyancy; F^x , F^y , and F^z represent the viscous forces in the x , y , and z directions, respectively. The small aspect ratio of most large-scale flows allows the term f^*w in the zonal momentum equation to be neglected in favor of fU since, by continuity

$$\frac{[f^*w]}{[fv]} \sim \frac{fW}{fU} \sim \frac{H}{L},$$

where for simplicity we have assumed $f \approx f^*$ and square brackets indicate scaling, W and U represent the order of magnitude of the vertical and horizontal velocities, H and L the vertical and horizontal scales, and $H \ll L$. In convective regimes, however, observations show that plumes have typical aspect ratio of order 1 ([Gascard and Clarke 1983](#)), implying that the f^*w term cannot be neglected.

Likewise, while the hydrostatic nature of the large-scale oceanic circulation allows the inertia and the rotational terms to be neglected in the vertical momentum equation, such an approximation is no longer valid during convective events (see, e.g., [Jones and Marshall 1993](#)). To determine the relative magnitude of the rotational term with respect to the inertia and advective ones the latter are scaled as the vertical advective term, which yields

$$\frac{[ww_z]}{[f^*u]} \sim \frac{W^2}{fUH} \sim \frac{W}{fH},$$

where we have made use of continuity and assumed aspect ratio 1 ($W \sim U$). Typical vertical velocities during convective events (e.g., [Schott et al. 1993](#)), are of the order of 10 cm s^{-1} , which gives the plumes a Rossby number of order 1:

$$W \sim 0.1 \text{ m s}^{-1}, \quad f \sim 10^{-4} \text{ s}^{-1}, \quad H \sim 1000 \text{ m},$$

making the two terms the same order of magnitude.

APPENDIX B

8. Lagrangian Analytical Model Solution

The Lagrangian equations of motion for a parcel of initial buoyancy b_0 and ZAM m_0 moving in a mean flow described by (3) (see [section 3](#)) are

$$\begin{aligned} \frac{d^2y}{dt^2} &= -f^2y + f\eta z - fm_0 \\ \frac{d^2z}{dt^2} &= f\eta y - (N^2 + f^*\eta)z + b_0 + f^*m_0, \end{aligned} \quad (\text{B1})$$

where $\mathfrak{T} = f^* - a/f$ is the meridional absolute vorticity. Provided $N^2f + a\mathfrak{T} > 0$, which is equivalent to requiring that the PV of the mean flow be positive, solutions to this system are bounded but oscillatory. The parcel, initially located at the origin ($\mathbf{x}(0) = 0$), is initially at rest and has no initial ZAM anomaly with respect to the mean flow, which corresponds to imposing that $m_0 = 0$. Solutions to (14) are

$$y(t) = y_p - a \frac{f\eta}{\Delta} \cos(\omega_1 t) + b \frac{\omega_1^2 - f^2}{\Delta} \cos(\omega_2 t) \quad (\text{B2})$$

$$z(t) = z_p + a \frac{\omega_1^2 - f^2}{\Delta} \cos(\omega_1 t) + b \frac{f\eta}{\Delta} \cos(\omega_2 t), \quad (\text{B3})$$

where

$$\omega_{1,2} = \frac{1}{\sqrt{2}} [N^2 + f^2 + f^* \eta \pm \sqrt{(N^2 - f^2 + f^* \eta)^2 + 4f^2 \eta^2}]^{1/2}$$

$$a = \frac{1}{\Delta} [f\eta y_p - (\omega_1^2 - f^2) z_p]$$

$$b = -\frac{1}{\Delta} [(\omega_1^2 - f^2) y_p + f\eta z_p],$$

and $\Delta = f^2 \eta^2 + (\omega_1^2 - f^2)$ is the normalization factor. These are analogous to those found by Emanuel (1983b), except for the contribution of the f^* terms and the presence of an equilibrium point. The latter, (y_p, z_p) , is found by imposing

$$B(y_p, z_p) = b_0 \quad \text{and} \quad M(y_p, z_p) = m_0,$$

which, given (3), yields

$$y_p = \frac{b_0 \eta - N^2 m_0}{N^2 f + \alpha \eta}, \quad z_p = \frac{f b_0 + m_0 \alpha}{N^2 f + \alpha \eta}.$$

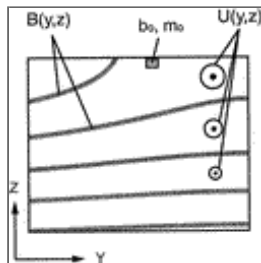
Tables

TABLE 1. Parameters for the numerical experiments

Exp	N, N_0 (10^3 s^{-1})	α (10^3 s^{-2})	f, f^* (10^3 s^{-1})	L (km)	L, H (km)	$Q \times 10^4$ (10^3 s^{-1})	f (10^3 s^{-1})
1	3, —	0	1.26, 0	—	—, 2	2	3
2	3, —	0	1.26, 0.33	—	—, 2	2	3
3	3, —	1	1.26, 0	—	—, 2	2	3
4	3, —	1	1.26, 0.33	—	—, 2	2	3
5	3, —	-1	1.26, 0.33	—	—, 2	2	3
6	21, 6	-2	1.26, 0.33	—	0.5, 2	2	3.5
7	3, 1	—	1.26, 0	5	0.5, 20	2	3

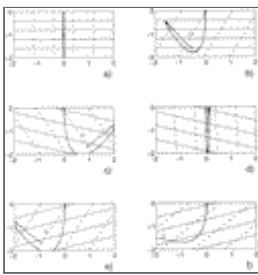
Click on thumbnail for full-sized image.

Figures



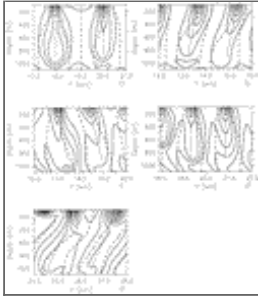
Click on thumbnail for full-sized image.

FIG. 1. Schematic of the Lagrangian model for a parcel of fluid (of buoyancy b_0 and zonal absolute momentum m_0) initially at the surface of a mean zonal flow $U(y, z)$ with buoyancy distribution $B(y, z)$



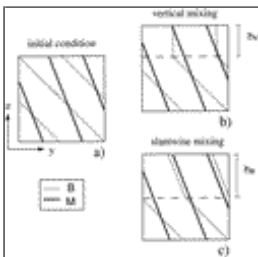
[Click on thumbnail for full-sized image.](#)

FIG. 2. Parcel trajectories (dotted line) plotted in the y - z plane (axes units are in kilometers). The equilibrium point is an open circle. ZAM surfaces are dashed (contour interval is 0.1 m s^{-1}) and isopycnals are solid (contour interval is $5 \times 10^{-6} \text{ m s}^{-2}$). Units for α are 10^{-8} s^{-2} and for f^* are 10^{-4} s^{-1} . (a) $\alpha = 0, f^* = 0$; (b) $\alpha = 0, f^* = 0.733$; (c) $\alpha = 1, f^* = 0$; (d) $\alpha = 1, f^* = 0.733$; (e) $\alpha = -1, f^* = 0$; (f) $\alpha = -1, f^* = 0.733$



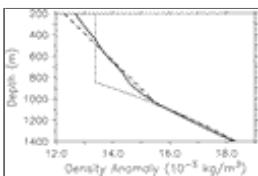
[Click on thumbnail for full-sized image.](#)

FIG. 3. Snapshots of plumes for (a) expt 1, (b) expt 2, (c) expt 3, (d) expt 4, and (e) expt 5. All snapshots were taken at the same time (after three days of surface forcing). Isopycnals are solid (contour interval $5 \times 10^{-6} \text{ m s}^{-2}$); ZAM surfaces dashed (contour interval is 0.1 m s^{-1}). The straight (solid) line overlaid on each plume is the analytical model prediction



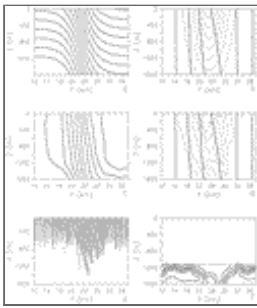
[Click on thumbnail for full-sized image.](#)

FIG. 4. Schematic showing contours of zonal absolute momentum, M , and buoyancy, B , initially (a) and after convection has occurred as a result of a surface buoyancy loss for (b) a vertical mixing scheme and (c) a slantwise mixing scheme



[Click on thumbnail for full-sized image.](#)

FIG. 5. Horizontally averaged density anomaly during convection in expt 6 (solid line). Overlaid are the one-dimensional model prediction (dotted) and the slantwise mixing model prediction (dashed)



Click on thumbnail for full-sized image.

FIG. 6. Initial (a) buoyancy (contour interval is $2 \times 10^{-5} \text{ m s}^{-2}$), and (b) zonal velocity (dashed; contour interval is 5 cm s^{-1}), and ZAM (solid; contour interval 0.5 cm s^{-1}) contours for expt 7. (c) as in (a) and (d) as in (b) for the end state. (e) Time-averaged (during convection) kinetic energy in the plumes' plane. (f) PV (contour interval is $2 \times 10^{-12} \text{ s}^{-2}$) in the end state; line overlaid is the one-dimensional mixing prediction

* Current affiliation: Woods Hole Oceanographic Institution, Woods Hole, Massachusetts

Corresponding author address: Fiammetta Straneo, Dept. of Physical Oceanography, WHOI, MS 21, Woods Hole, MA 02543. E-mail: fstraneo@whoi.edu

top ▲



© 2008 American Meteorological Society [Privacy Policy and Disclaimer](#)
 Headquarters: 45 Beacon Street Boston, MA 02108-3693
 DC Office: 1120 G Street, NW, Suite 800 Washington DC, 20005-3826
amsinfo@ametsoc.org Phone: 617-227-2425 Fax: 617-742-8718
[Allen Press, Inc.](#) assists in the online publication of AMS journals.